ISSN 1070-3284, Russian Journal of Coordination Chemistry, 2024, Vol. 50, No. 4, pp. 246–256. © Pleiades Publishing, Ltd., 2024.

Influence of the Coordination Environment on the EPR Spectra of Mononuclear Gd Thiocyanates

S. P. Petrosyants[a], A. B. Ilyukhin[a], K. A. Babeshkin[a], E. A. Ugolkova[a], V. V. Minin[a], P. S. Koroteev[a, *], and N. N. Efimov[a]

[a] *Kurnakov Institute of General and Inorganic Chemistry, Russian Academy of Sciences, Moscow, 119991 Russia*

**e-mail: pskoroteev@list.ru*

Received October 25, 2023; revised December 10, 2023; accepted December 11, 2023

Abstract—Using the synthesized salt $Gd(NCS)_3 \cdot 6H_2O$, previously unknown mononuclear molecular complexes $[Gd(H_2O)(bpy)_2(NCS)_3] \cdot 0.5(bpy) \cdot H_2O$, $[Gd(H_2O)(phen)_2(NCS)_3] \cdot phen \cdot 0.5H_2O$ as well as ionic ones $[Hbpy][Gd(NCS)_4(bpy)_2] \cdot H_2O$, $[Hphen][Gd(NCS)_4(phen)_2]$ (bpy is 2,2'-bipyridine, phen is 1,10-phenanthroline) were prepared. Structural characteristics of the obtained compounds were determined using X-ray diffraction data. The magnetic susceptibility and EPR data of the new Gd complexes are considered taking into account the features of their composition and structure. Due to the peculiarities of the electronic structure, Gd complexes can serve as test systems for analyzing the field strength of ligands and the geometry of the local environment of the 4*f*-metal ion. It is shown that EPR spectroscopy is highly efficient method for determining the spin Hamiltonian parameters and, consequently, for characterizing the local environment of the gadolinium ion in complexes. However, the EPR method does not allow one to determine the sign of the splitting parameter in the zero field *D*, which requires additional studies.

Keywords: Gd thiocyanates, bipyridine, phenanthroline, X-ray diffraction analysis, EPR, magnetism

DOI: 10.1134/S1070328423601413

INTRODUCTION

In recent years, heteroleptic lanthanide thiocyanates have been comprehensively studied due to a variety of useful properties, namely, slow relaxation of magnetization (single-molecule magnet properties) [1–5], luminescence [6–8], and biological activity [7]. In addition, thiocyanate derivatives of lanthanides with alkylimidazolium cations are of interest as ionic liquids [9, 10]. Such a wide range of potential applications obviously originates from the possibility of fine-tuning the structure of these complexes. Indeed, though almost all known Ln thiocyanates are mononuclear complexes and their structural variety is actually equal to the variety of auxiliary ligands, methods of varying not only the composition of the ligands but also the complex charge, are developed. For instance, there are molecular [3, 4, 11, 12] and anionic [3, 13–15] thiocyanate complexes known to date. The configuration of the Ln^{3+} environment, i.e., its qualitative and quantitative composition as well as mutual location of the different donating centers varies widely for these compounds thus being one of the essential factors that govern all the mentioned properties.

Among the studies of Ln thiocyanates, ones dealing with their SMM behavior are of undoubted interest since slow relaxation of the magnetization allows one to assume their possible applications in molecular spintronics and high-density magnetic memory devices [16–19]. Similarly to other Ln complexes, the vast majority of thiocyanate SMMs is those formed by Dy^{3+} due to favorable features of the electronic structure of that ion, namely, bistability of its ground state and significant magnetic anisotropy [3, 20–22]. However, currently known number of Dy-based thiocyanate SMMs is still scarce and further investigation in order to design the most effective thiocyanate based SMMs is required. In addition to the experimental studies of magnetic relaxation, the search of possible empirical patterns in order to predict the efficiency of particular SMM, i.e., to evaluate its magnetic anisotropy, is worth conducting.

EPR spectroscopy is a very effective method for determining the parameters of the spin Hamiltonian and, consequently, for characterizing the local environment of Gd^{3+} ion in complexes. Due to the peculiarities of the electronic structure, it is possible to record highly informative EPR spectra with a well-resolved fine structure (if any) for Gd complexes at room temperature already, which makes it possible to use them as test systems for analyzing the strength of the ligand field and the geometry of the local environment of the metal ion.

Among the promising correlations, there is one between the magnetic anisotropy of complexes formed

by Dy^{3+} and the features of EPR behavior, namely, the value of D and E (zero-field splitting parameters) for their Gd^{3+} analogs. The possibility of such correlations originates from highly-detailed, fingerprint-like EPR spectra for Gd^{3+} which, in turn, is governed by ZFS of the $S = 7/2$ ground state [23]. Such a correlation was shown to be actual for $[Ln(Cp^{ttt})_2][B(C_6F_5)_4]$ ($Cp^{ttt} = C_5H_2{}^tBu_3$-1,2,4) complexes [24]. The mentioned study involves the Dy-based compound exhibiting the highest known barrier of the magnetization reversal [25], i.e. it is descriptive of the magnetic anisotropy which is in good correspondence with D for Gd complex. However, such investigations are still scarce and further ones are thus required in order to find out the limits of applicability. In addition, possible correlation has a physical sense only when isomorphic complexes are being considered, i.e., there should be absolutely similar qualitative and quantitative composition both in coordinated ligands and in solvated molecules. Since each particular series of thiocyanate complexes formed by different Ln almost always meets this requirement [4, 12–15, 26], it is worth investigating these compounds in order to find out possible correlations.

Due to the large number of parameters to be taken into account when constructing reliable correlations of this kind (the geometry of the coordination environment of the central ion, the strength of the ligand field, the relative position of the ligands, etc.), it is necessary to accumulate sufficient amount of experimental material. This work is one of first works on the search for possible correlations between the parameters of the spin Hamiltonian of Gd complexes and the parameters of slow magnetic relaxation in isostructural dysprosium complexes.

In this work, an attempt was made to search for possible correlations between the parameters of the spin Hamiltonian obtained from EPR spectroscopy data at room temperature and slow magnetic relaxation in Gd complexes which are isomorphic with Dy ones [3] for the entire series of thiocyanate complexes with bidentate chelating N-donors, 2,2'-bipyridine (bpy) and 1,10-phenanthroline (phen).

EXPERIMENTAL

The following commercial reagents and solvents were used: Gd_2O_3, bpy and phen (Aldrich), $Ba(NCS)_2 \cdot 3H_2O$, aqueous H_2SO_4 (standard titer solution), EtOH. All the substances were used as purchased. All the operations were carried out on the air.

Synthesis of $Gd(NCS)_3 \cdot 6H_2O$ (I), $[Gd(H_2O)(bpy)_2(NCS)_3] \cdot 0.5(bpy) \cdot H_2O$ (II), $[Gd(H_2O)(phen)_2(NCS)_3] \cdot phen \cdot 0.5H_2O$ (III), $[Hbpy][Gd(NCS)_4(bpy)_2] \cdot H_2O$ (IV), and $[Hphen][Gd(NCS)_4(phen)_2]$ (V).

All the complexes were prepared according to previously developed procedures [3, 6]. The sample of $Gd(NCS)_3 \cdot 6H_2O$ (**I**) with the crystals suitable for structural studies was isolated as the only product of the interaction between Gd_2O_3 and aqueous HNCS. The single-phase state of the sample was confirmed by powder XRD (Fig. S1). Compounds $[Gd(H_2O)(bpy)_2(NCS)_3] \cdot 0.5(bpy) \cdot H_2O$ (**II**) and $[Gd(H_2O)(phen)_2(NCS)_3] \cdot phen \cdot 0.5H_2O$ (**III**) were isolated from the ethanolic solutions containing ≈0.5 mmol of compound **I** and 1.5 mmol of corresponding ligand, bpy (for **II**) or phen (for **III**). The yields were 0.31 g (0.409 mmol, 82% basing on Gd) for **II** and 0.18 g (0.200 mmol, 40% basing on Gd) for **III**. The single-phase state of the samples was confirmed by powder XRD (Figs. S2, S3).

Ionic complexes $[Hbpy][Gd(NCS)_4(bpy)_2] \cdot H_2O$ (**IV**) and $[Hphen][Gd(NCS)_4(phen)_2]$ (**V**) were isolated from water-ethanolic solutions containing HNCS (ca. 0.5 mmol), bpy or phen, respectively (ca. 1.5 mmol) and **I** (ca. 0.5 mmol) after evaporation during several days. The yields were 0.187 g (0.213 mmol, 43% basing on Gd) and 0.356 g (0.382 mmol, 78% basing on Gd) for **IV** and **V**, respectively. The single-phase state of the samples was confirmed by powder XRD (Figs. S4, S5).

ATR-IR for **I** (ν, cm^{-1}): 3295 s, 2870 w, 2079 s, 1638 m, 1618 m, 1606 m, 1529 m, 1500 m, 1433 m, 943 w, 783 w, 592 s, 483 s, 440 vs.

For $C_{28}H_{24}N_8O_2S_3Gd$ (**II**)

Anal. calcd., %	C, 44.37	H, 3.19	N, 14.78	S, 12.69
Found, %	C, 43.91	H, 2.89	N, 14.08	S, 13.49

ATR-IR for **II** (ν, cm^{-1}): 3402 m, 3666 m, 3105 w, 3074 m, 3053 m, 2087 m, 2055 s, 1619 w, 1595 s, 1572 m, 1562 m, 1493 m, 1473 m, 1456 m, 1435 s, 1420 m, 1314 m, 1280 w, 1253 w, 1240 m, 1218 m, 1177 m, 1156 m, 1116 w, 1100 m, 1065 m, 1042 w, 1011 s, 980 m, 966 m, 906, 896 w, 855 m, 812 w, 765 s, 756 vs, 736 vs, 644 s, 624 s, 602 m, 572 m, 555 m, 540 m, 487 m, 474 m, 433 m, 415 s.

For $C_{39}H_{27}N_9O_{1.5}S_3Gd$ (**III**)

Anal. calcd., %	C, 52.10	H, 3.03	N, 14.02	S, 10.70
Found, %	C, 51.90	H, 2.89	N, 13.69	S, 10.85

ATR-IR for **III** (ν, cm^{-1}): 3329 w, 3974 w, 3060 w, 3050 w, 2042 s, 2004 m, 1623 m, 1589 m, 1573 m, 1518 m, 1495 m, 1449 m, 1449 w, 1420 s, 1342 m, 1299 w, 1256 w, 1221 w, 1206 w, 1140 m, 1102 m, 1090 m, 1052 w, 1042 w, 984 w, 971 w, 949 w, 891 w,

864 m, 843 vs, 768 m, 722 vs, 637 m, 626 m, 554 w, 489 m, 463 w, 455 w, 433 w, 416 m.

For $C_{34}H_{27}N_{10}OS_4Gd$ (**IV**)

Anal. calcd., %	C, 46.56	H, 3.10	N, 15.97	S, 14.62
Found, %	C, 46.26	H, 2.65	N, 15.26	S, 13.62

ATR-IR for **IV** (ν, cm^{-1}): 3077 m, 3053 m, 3040 m, 3018 m, 2043 s, 2001 m, 1626 m, 1616 m, 1593 s, 1583 m, 1573 m, 1524 m, 1490 m, 1470 m, 1457 m, 1431 s, 1355 m, 1323 m, 1308 m, 1273 m, 1242 m, 1221 m, 1171 m, 1151 m, 1114 m, 1099 m, 1088 m, 1062 m, 1044 m, 1011 s, 994 m, 977 m, 967 m, 930 m, 898 m, 879 m, 806 m, 756 vs, 735 s, 721 s, 651 m, 643 m, 609 m, 551 w, 542 w, 504 w, 490 m, 481 m, 443 m, 415 s.

For $C_{40}H_{25}N_{10}S_4Gd$ (**V**)

Anal. calcd., %	C, 51.59	H, 2.70	N, 15.04	S, 13.77
Found, %	C, 51.61	H, 2.98	N, 14.97	S, 13.35

ATR-IR, for **V** (ν, cm^{-1}): 3091 m, 3050 m, 3013 m, 2086 m, 2041 s, 2002 m, 1626 m, 1613 w, 1589 m, 1572 m, 1535 m, 1517 m, 1493 m, 1465 m, 1449 w, 1419 s, 1364 m, 1340 m, 1316 m, 1297 w, 1280 w, 1252 w, 1232 m, 1218 m, 1184 m, 1148 w, 1137 m, 1102 m, 1090 m, 1068 w, 1037 w, 991 w, 974 w, 966 w, 919 w, 885 w, 862 m, 840 vs, 823 m, 769 m, 726 s, 717 vs, 636 m, 619 w, 606 w, 598 w, 552 w, 538 w, 486 m, 462 w, 435 w, 416 w.

X-ray diffraction analysis. Experimental single crystal X-ray diffraction data for **I** were collected on a Bruker SMART APEX2 instrument [27]. Absorption was taken into account by a semiempirical method based on equivalents using SADABS [28]. The structure was determined using a combination of the direct methods and Fourier syntheses. The positions of H atoms were localized from differential Fourier syntheses. The structure was refined by the full-matrix anisotropic-isotropic (H atoms) least squares method. All the calculations were carried out using SHELXS and SHELXL software [29].

The powder X-ray diffraction patterns were measured with a Bruker D8 ADVANCE X-ray diffractometer (CuK_α, Ni filter, LYNXEYE detector, reflection geometry). The Rietveld refinement was carried out using models of isostructural Eu or Y analogues of complexes **II**–**V** [8, 30]. All calculations were carried out using the TOPAS program [31]. Crystallographic data and refinement parameters for structures **I**–**V** are shown in Tables S1, S2.

The experimental data for the newly characterized compounds **I**–**IV** were deposited with the Cambridge Crystallographic Data Centre (CCDC 2329216–2329219, respectively). These data can be obtained, free of charge, via http://www.ccdc.cam.ac.uk/conts/retrieving.html, or e-mail: deposit@ccdc.cam.ac.uk. X-ray diffraction studies were performed at the Centre of Shared Equipment of IGIC RAS.

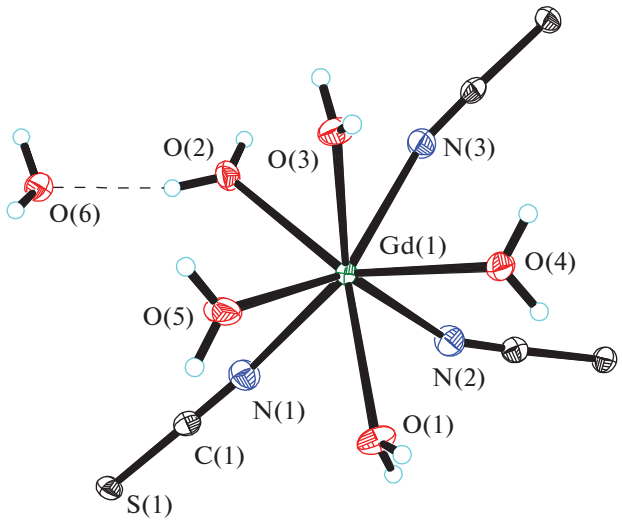

Fig. 1. Fragment of structure **I**.

Elemental analyses were carried out using standard techniques on a EUROEA 3000 analyzer.

Attenuated total reflection IR spectra (ATR-IR) were recorded on Fourier spectrometer Bruker ALPHA equipped with a diamond tool in the range of 400–4000 cm^{-1}.

Magnetic susceptibility measurements were performed using a Quantum Design PPMS-9 susceptometer. This instrument works in the temperature range of 2–300 K under the applied dc fields up to 9 T. The paramagnetic components of the magnetic susceptibility χ were determined taking into account diamagnetic contribution evaluated from Pascal's constants and the contributions of the sample holder and mineral oil.

EPR spectra were recorded using an ELEXSYS E-680X EPR spectrometer in the X-band (9.8 GHz) at a temperature of 293 K. The methodology used for calculating resonant fields and transition intensities by means of the Belford method [32] is briefly described in the work [33].

RESULTS AND DISCUSSION

The salt $Gd(NCS)_3 \cdot 6H_2O$ synthesized by us is isostructural with analogous derivatives of Y [32], Eu, Tb [6] and Dy [3]. It is a neutral complex $[Gd(H_2O)_5(NCS)_3]$ with one water molecule in the outer sphere (Fig. 1). As well as in isostructural analogues, in complex **I** CN of Gd is 8, the coordination site is GdO_5N_3.

The interaction of **I** with bidentate heterocyclic ligands (bpy/phen) at a reagent ratio of 1 : 3 in an eth-

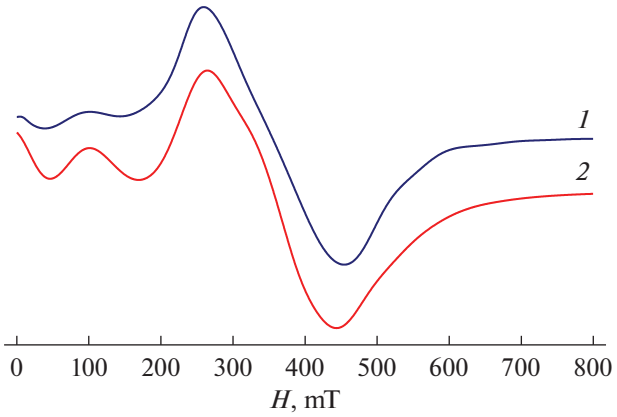

Fig. 2. Experimental EPR spectrum of complex **I** (*1*) and its theoretical approximation (*2*) with the following SH parameters: $D = 0.007$ cm^{-1}, $E = 0.002$ cm^{-1}, $B_4^0 = -0.0003$ cm^{-1}, $g = 1.999$.

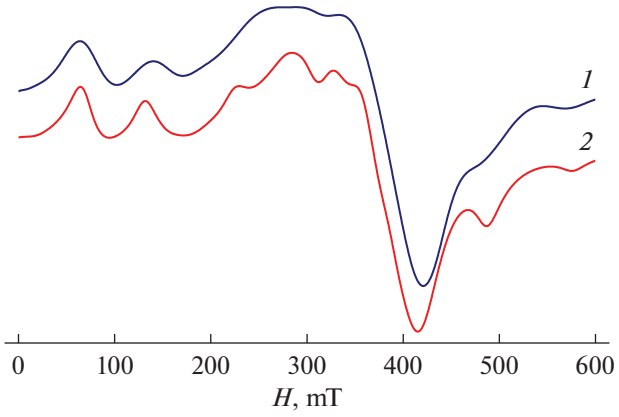

Fig. 3. Experimental EPR spectrum of complex **II** (*1*) and its theoretical approximation (*2*) with the following SH parameters: $D = 0.04958$ cm^{-1}, $E = 0.0056$ cm^{-1}, $B_4^0 = -2.6 \times 10^{-5}$ cm^{-1}, $B_6^0 = 3 \times 10^{-7}$ cm^{-1}, $g = 1.989$.

anol solution brings about formation of neutral complexes **II** and **III**. Powder X-ray diffraction analysis confirmed their isostructurality with the corresponding complexes $[Y(H_2O)(bpy)_2(NCS)_3]\cdot 0.5(bpy)\cdot H_2O$ and $[Eu(H_2O)(phen)_2(NCS)_3]\cdot phen\cdot 0.5H_2O$ [8], respectively (Figs. S1–S5). In complexes **II** and **III**, the CN of Gd is 8, the coordination site is $GdON_7$, one coordinated water molecule is retained in the coordination sphere. A feature of these neutral complexes is the presence of corresponding N-donor and water molecules in the outer coordination sphere.

Anionic complexes **IV** and **V** were obtained from ethanolic solutions containing $Gd(NCS)_3\cdot 6H_2O$, three equivalents bpy or phen, and HNCS. Powder X-ray diffraction showed their isostructurality with the corresponding yttrium complexes (Figs. S4, S5) [8]. The coordination sphere of **IV** and **V** is formed of two diimine molecules and four NCS anions, CN of Gd is 8, the coordination site is GdN_8. The charge of the complexes is compensated by the protonated diamine molecule ($[Hbpy]^+$ or $[Hphen]^+$).

Structure of **I** belongs to isostructural series $[Ln(H_2O)_5(NCS)_3]\cdot H_2O$ (Ln = Y [34]; Eu, Tb [6]) and contains molecular complexes $[Gd(H_2O)_5(NCS)_3]$ and crystallization water molecules (Fig. 1). The polyhedron of the Gd atom is average between a square antiprism and a two-capped triangular prism.

The molecular and crystalline structures of compounds **II**–**V** are similar to those of their isostructural analogs. Compounds **II** and **III** are isostructural with Y [8] and Nd [35] analogs and Eu [8] complexes, respectively. Complex **IV** is isostructural with Y [30], Eu [8] and Dy [3] analogs. Complex **V** was first described in the work [36], the Ce [7], Nd [37], and Y [30] derivatives are isostructural with it.

EPR study of the complexes (I–V). The EPR spectra of complexes **I**–**V** were recorded using the solid polycrystalline samples (Figs. 2–6). The experimental EPR spectra of Gd(III) complexes are very diverse and highly informative. The reverse side of the high information content of the spectra is the non-triviality of their interpretation. The only way to interpret such spectra is to simulate the theoretical spectrum with a certain set of parameters of the spin Hamiltonian (SH), which represents the expansion of the crystal field into multipoles, and to reach the match of the simulated spectrum with the experimental one by means of parameters variation. For mathematical modeling of the EPR spectra of Gd^{3+} ($S = 7/2$) complexes, to take into account splitting in a zero field, it is necessary to consider not only the quadratic, the so-called "quadrupole," components of the fine interaction tensor but also the components of higher orders, the fourth and sixth ones. However, it is difficult to take into account all the terms of the crystal field, since the number of terms in a low-symmetry environment is very large. When modeling spectra, it was necessary to take into account terms of the fourth and sixth order and, if possible, reduce their number. To achieve this goal, two simplifying assumptions were made. First, it was assumed that one of the main axes of the second-order tensor was simultaneously a fourth- and sixth-order axis, and second, if a high-spin ion was in a cubic environment, then the Z axis of the second-order tensor coincided with the fourth-order axis of the cube.

Under such conditions, the spin Hamiltonian (SH) is mainly affected by quadrupole terms and higher-order diagonal terms, as well as contributions from the cubic environment.

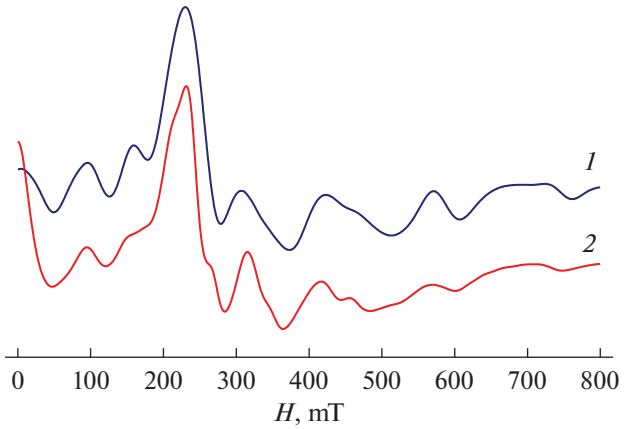

Fig. 4. Experimental EPR spectrum of complex **III** (*1*) and its theoretical approximation (*2*) with the following SH parameters: $D = 0.092$ cm^{-1}, $E = 0.0089$ cm^{-1}, $B_4 = 2.0 \times 10^{-5}$ cm^{-1}, $B_6 = 2 \times 10^{-7}$ cm^{-1}, $g = 1.99$.

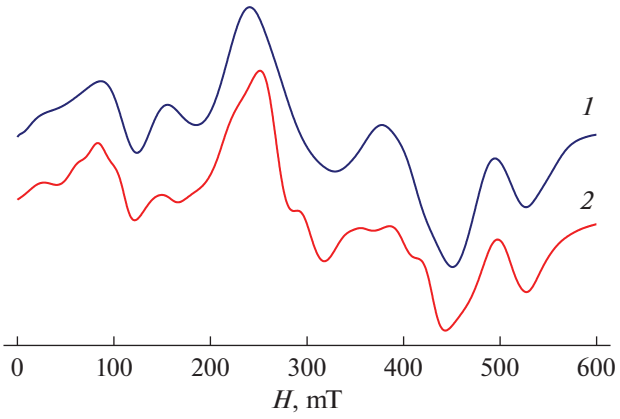

Fig. 5. Experimental EPR spectrum of complex **IV** (*1*) and its theoretical approximation (*2*) with the following SH parameters: $D = 0.0694$ cm^{-1}, $E = 0.0072$ cm^{-1}, $B_4 = 2.0 \times 10^{-5}$ cm^{-1}, $B_6 = 2 \times 10^{-7}$ cm^{-1}, $g = 1.99$.

$$H = g\beta(S_xH_x + S_yH_y + S_zH_z) + D \times \left(S_z^2 - \frac{1}{3}S(S+1)\right) + E(S_x^2 - S_y^2) + B_4^0O_4^0 + B_6^0O_6^0 + B_4(O_4^0 + 5O_4^4) + B_6(O_6^0 - 21O_6^4),$$

where O_k^q are the equivalent spin Stevens operators, B_k^q are the Stevens parameters describing the expansion of the crystal field into multipoles, ($D = 3B_2^0$, $E = B_2^2$) are the second-order Stevens operators.

In compounds **II** and **V**, it is possible to achieve qualitative agreement with the experimental spectrum when quadrupole interactions and additional axial splittings of the fourth and sixth orders are taken into account (for compound **I**, only the axial axis of the fourth order). In compounds **III** and **IV**, the best agreement is achieved when the cubic field of the fourth and sixth orders distorted by the quadrupole interaction along the fourth order axis is taken into account.

SH was diagonalized numerically. Calculations of the resonant fields of spin Hamiltonians for building of the theoretical spectrum were carried out using the Belford method (eigenfield method) [32].

The Gd^{3+} ion in an isotropic environment and without a magnetic field has an octet of unsplit levels. In a crystal field of low symmetry, the maximum possible splitting is into four doublets. The energy gap between the lowest and highest energy doublets can be taken as a measure of the asymmetry of the environment. To determine the energy of doublets, it is necessary to solve the SH determinant in the basis of states with different projections of the total spin on the Z axis (M_s).

$$H\left(\pm\frac{1}{2},\pm\frac{1}{2}\right) = -5D + 9\times60(B_4^0 + B_4) - 5\times1260(B_6^0 + B_6),$$
$$H\left(\pm\frac{3}{2},\pm\frac{3}{2}\right) = -3D - 3\times60(B_4^0 + B_4) + 9\times1260(B_6^0 + B_6),$$
$$H\left(\pm\frac{5}{2},\pm\frac{5}{2}\right) = D - 13\times60(B_4^0 + B_4) - 5\times1260(B_6^0 + B_6),$$
$$H\left(\pm\frac{7}{2},\pm\frac{7}{2}\right) = 7D + 7\times60(B_4^0 + B_4) + 1260(B_6^0 + B_6),$$

$$H\left(\pm\frac{1}{2},\pm\frac{5}{2}\right) = 3\sqrt{5}E \qquad H\left(\pm\frac{1}{2},\mp\frac{7}{2}\right) = 60\sqrt{35}B_4 - 21\times3\times60\sqrt{55}B_6,$$
$$H\left(\pm\frac{1}{2},\mp\frac{3}{2}\right) = 2\sqrt{15}E \qquad H\left(\pm\frac{3}{2},\mp\frac{5}{2}\right) = 300\sqrt{3}B_4 + 21\times7\times60\sqrt{3}B_6,$$
$$H\left(\pm\frac{3}{2},\pm\frac{7}{2}\right) = \sqrt{21}E.$$

Table 1. Energy of Gd^{+3} doublets in the crystal field for complexes **I**–**V** (cm^{-1}). The second-fifth columns refer to doublets without taking into account off-diagonal members of the SH. Columns six through nine contain the energies of doublets, taking into account the off-diagonal terms of the SH. The tenth column contains the maximum spread of doublets in energy

	$H(\pm0.5, \pm0.5)$	$H(\pm1.5, \pm1.5)$	$H(\pm2.5, \pm2.5)$	$H(\pm3.5, \pm3.5)$	**1**	**2**	**3**	**4**	Δ
I	–0.197	0.033	0.241	–0.077	–0.198	0.0348	0.2414	–0.0778	0.4400
II	–0.2638	–0.1407	0.0680	0.3365	–0.2707	–0.1509	0.0880	0.3337	0.6044
III	–0.4505	–0.2773	0.0751	0.6527	–0.4150	–0.3570	0.1268	0.6452	1.0602
IV	–0.3375	–0.2095	0.0525	0.4945	–0.3374	–0.2374	0.0832	0.4916	0.8290
V	–0.2639	–0.1400	0.06581	0.3381	–0.2589	–0.1523	0.0750	0.3361	0.5950

The eighth order determinant is split into two fourth order determinants. Solving the equations, we obtain the energies of doublets in the zero field.

$$\begin{vmatrix} H\left(\pm\frac{1}{2},\pm\frac{1}{2}\right)-E & H\left(\pm\frac{1}{2},\mp\frac{3}{2}\right) & H\left(\pm\frac{1}{2},\pm\frac{5}{2}\right) & H\left(\pm\frac{1}{2},\mp\frac{7}{2}\right) \\ H\left(\pm\frac{1}{2},\mp\frac{3}{2}\right) & H\left(\mp\frac{3}{2},\mp\frac{3}{2}\right)-E & H\left(\mp\frac{3}{2},\pm\frac{5}{2}\right) & H\left(\pm\frac{3}{2},\pm\frac{7}{2}\right) \\ H\left(\pm\frac{1}{2},\pm\frac{5}{2}\right) & H\left(\mp\frac{3}{2},\pm\frac{5}{2}\right) & H\left(\pm\frac{5}{2},\pm\frac{5}{2}\right)-E & 0 \\ H\left(\pm\frac{1}{2},\mp\frac{7}{2}\right) & H\left(\pm\frac{3}{2},\pm\frac{7}{2}\right) & 0 & H\left(\mp\frac{7}{2},\mp\frac{7}{2}\right)-E. \end{vmatrix}$$

For the complexes, the doublet energies are given in the Table 1. The doublet energies are given without and with off-diagonal elements. When the main contribution to the splitting is made by D, the energies of the doublets either increase monotonically or decrease with increasing modulus M_s. However, for complex **I**, B_4^0 makes the main contribution to the splitting. Complex **III** has the maximum value of the energy gap, which corresponds to the maximum value of D. However, in all complexes the rhombic distortion E is present, which leads to a mixing of states with different values of the projections of the total spin on the Z axis, and can facilitate the direct transition during magnetic relaxation without overcoming the potential barrier at negative D.

For complex **III**, slow magnetic relaxation is not observed (see AC-magnetization section), which may be due to the large value of E parameter, which indicates a high probability of direct relaxation of the magnetization (transition between $\pm7/2 <-> \pm1/2$ states).

It should be specially emphasized that CW-EPR spectroscopy at room temperarure does not allow one to determine the sign of D parameters for Gd, but allows one to determine their absolute values only. To determine the sign of the splitting parameters in a zero field, it is necessary to carry out additional studies,

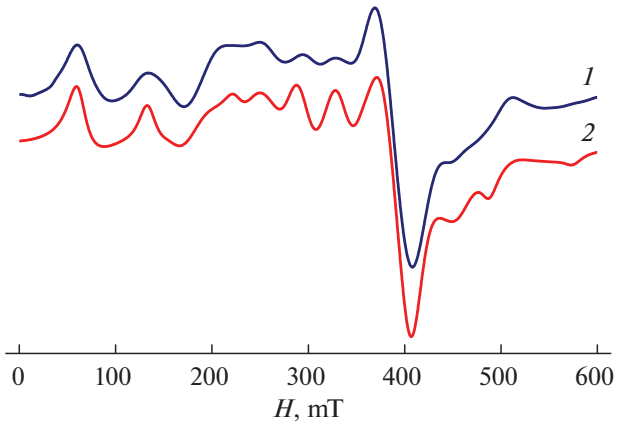

Fig. 6. Experimental EPR spectrum of complex **V** (*1*) and its theoretical approximation (*2*) with the following SH parameters: $D = 0.04967\ cm^{-1}$, $E = 0.00187\ cm^{-1}$, $B_4^0 = -2.4 \times 10^{-5}\ cm^{-1}$, $B_6^0 = 4.1 \times 10^{-7}\ cm^{-1}$, $g = 1.989$.

Table 2. Characteristics of the complexes **I**–**V** obtained by approximation of dc-magnetic measurements data using PHI software [38] ($\chi_m T$, *g*-factors (*g*), zero-field splitting parameters (*D*), inter molecular interaction parameter (*zJ*))

	$\chi_m T$, cm^3 K mol^{-1}		*g*		*D*, cm^{-1}		*zJ*, cm^{-1}	
	300 K	2 K	*D* < 0	*D* > 0	*D* < 0	*D* > 0	*D* < 0	*D* > 0
I	7.92	5.53	2.00(8)	2.01(3)	−1.046	2.200	0.0086	0.0086
II	8.19	6.74	2.03(4)	2.04(1)	−2.725	2.298	0.0335	0.0177
III	7.59	3.78	1.97(1)	1.97(5)	−1.200	2.401	−0.0108	−0.0105
IV	8.09	6.93	2.01(9)	2.02(8)	−3.045	0.710	0.0376	0.0057
V	8.17	6.70	2.03(1)	2.03(5)	−2.682	2.700	0.0329	0.0208

such as, for example, measurements of the dynamic magnetic susceptibility (see the AC-magnetization section below).

On a basis of the obtained values of the spin Hamiltonian parameters of the complexes **I**–**V** and their comparison with the values of the magnetization reversal energy barrier for the isostructural dysprosium complexes [3], we can conclude that to observe the most effective slow magnetic relaxation in Dy complexes having a similar structure, and therefore the similar influence of force fields, as well as the relative location of the ligands, it is necessary that the values of the SG parameters of Gd complexes should be in the ranges determined by the following values: $D > 0.06$; $E < 0.008$ cm^{-1}. To clarify the boundaries of admissible parameter values, a significant expansion of the range of objects in research of this kind is required.

DC magnetic properties of the complexes (I–V). Magnetic properties of the complexes were investigated under 5000 Oe dc-magnetic field. The $\chi_m T$ values at 300 K for complexes **I**–**V** are close to the theoretical one 7.88 cm^3 K mol^{-1} for an isolated single Gd^{3+} ion (Table 2). The values of $\chi_m T$ for mononuclear complexes remains virtually constant down to 12 K and decreases sharply upon reaching 6 K (Fig. 7).

Such behavior is apparently associated with weak intermolecular antiferromagnetic interactions between Gd^{3+} ions. It is known that in the solid state the molecular magnetic centers, even if they are well

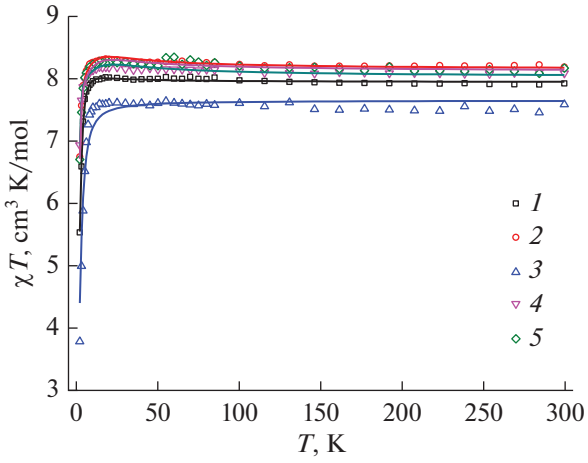

Fig. 7. Plots of $\chi_m T$ vs. temperature for mononuclear complexes **I**–**V** in 5000 Oe dc field. The lines show the best fit of the theoretical model to the experimental data for Gd compounds using PHI.

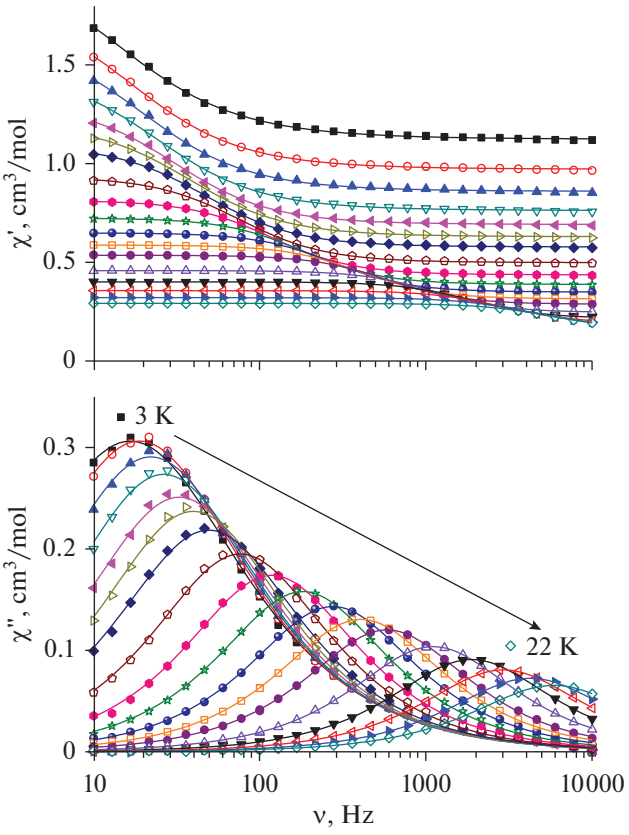

Fig. 8. Frequency dependencies of the real (χ', top) and imaginary (χ'', bottom) components of the ac susceptibility between 3 and 22 K for **I** in 1500 Oe dc-field. Solid lines are guides for eyes (χ'), fittings of experimental data by the generalized Debye model (χ'').

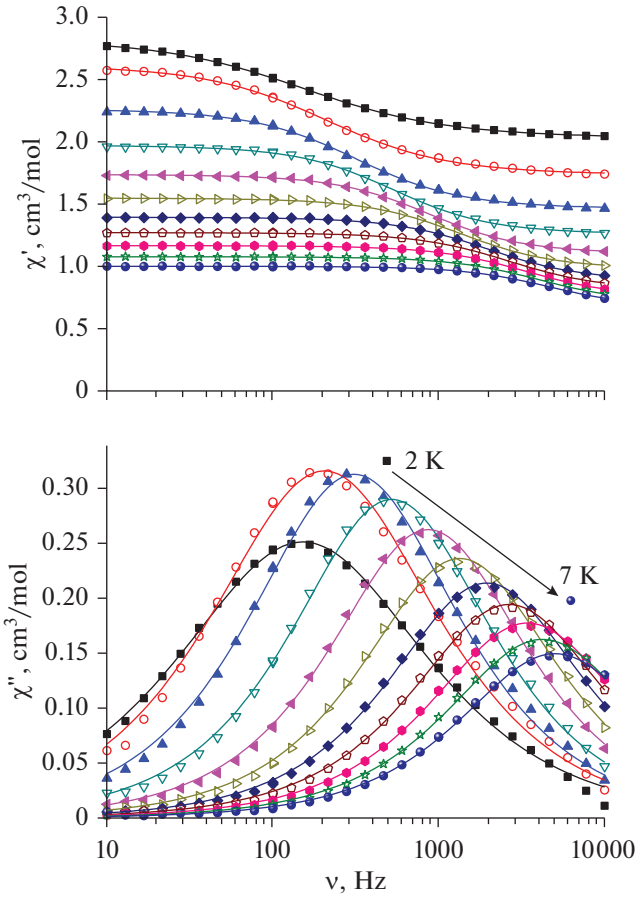

Fig. 9. Frequency dependencies of the real (χ', top) and imaginary (χ", bottom) components of the ac susceptibility between 2 and 7 K for **II** in 1000 Oe dc-field. Solid lines are guides for eyes (χ'), fittings of experimental data by the generalized Debye model (χ").

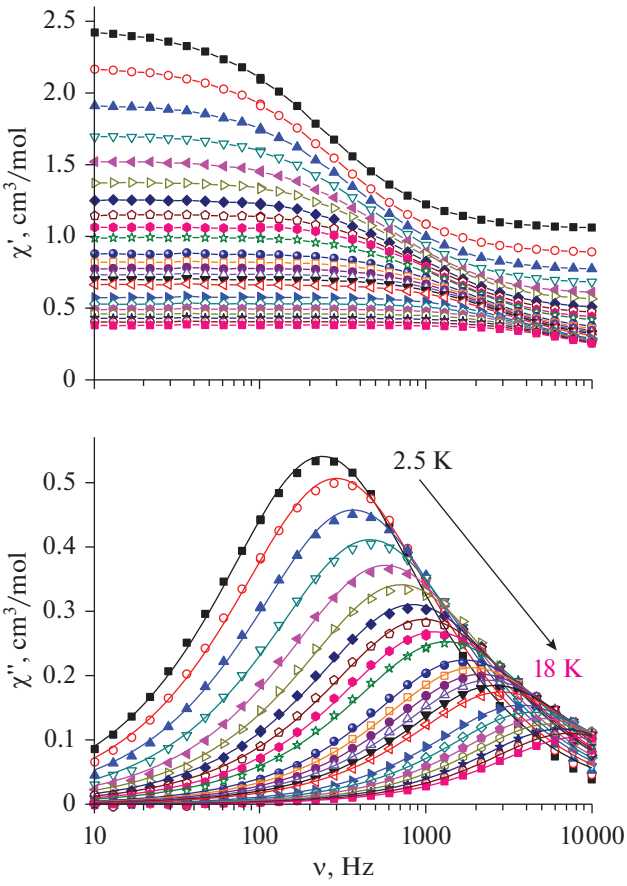

Fig. 10. Frequency dependencies of the real (χ', top) and imaginary (χ", bottom) components of the ac susceptibility between 2.5 and 18 K for **V** in 1500 Oe dc-field. Solid lines are guides for eyes (χ'), fittings of experimental data by the generalized Debye model (χ").

separated from each other, are rarely perfectly isolated from a magnetic point of view.

In order to estimate the value of the magnetic interactions in **I**–**V**, the temperature dependence of the χT product of **I**–**V** was fitted using the PHI program developed by N.F. Chilton et al. [38]. Approximation was carried out both for the case of setting the initial values of the parameter $D > 0$, and for $D < 0$. The best approximation parameters are given in Table 2. It should be noted that the approximation of the data of magnetic measurements is a very rough estimate of the spin Hamiltonian parameters (in contrast to EPR spectroscopy) due to the absence of any characteristic details. As a result, the addition of approximation parameters similar to those obtained from the analysis of EPR data leads to over-parametrization. The values of the zero-field splitting parameter D for Gd complexes obtained from the analysis of magnetic data cannot be regarded as reliable and one can only speak of a greater or lesser degree of distortion of the local environment of the Gd^{3+} ion.

AC magnetic properties. For better understanding of magnetic properties of complexes **I**–**V**, measurements in ac-magnetic field were performed and the plots of dependences of in-phase (χ') and out-of-phase (χ") magnetic susceptibility from frequency (ν) were obtained. In particular, dynamic magnetic behavior in magnetic fields from 0 to 5000 Oe was investigated (Figs. S6–S10). In zero dc-magnetic field, no significant signals on χ"(ν) were observed at 2 K. However, under the appliance of non-zero dc-fields the χ" values became significant, because of QTM suppression.

Optimal dc-fields are: for **I** and **V**, 1500 Oe; for **II** and **IV**, 1000 Oe (Figs. S6, S7, S9, S10). For complex **III**, the frequencies, corresponding to peak centers, are on the edge or beyond the sensitivity of magnetometer (Fig. S8). After finding the values of optimal dc-fields, the χ'(ν) and χ"(ν) isotherms for complexes **I**, **II**, **IV**, **V** (Figs. 8, 9, 10, S11) were approximated by the generalized Debye model yielding temperature dependences of relaxation time, $\tau(1/T)$ shown in Figs. 11, 12, S12, 13.

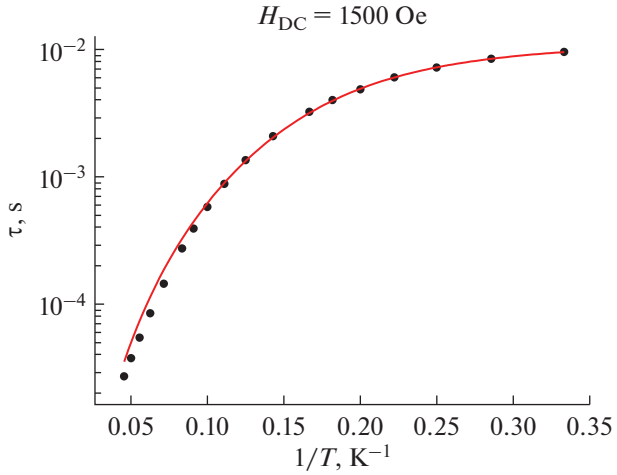

Fig. 11. The dependence of τ vs. $1/T$ for complex **I** under 1500 Oe dc-field. The solid red line is an approximation by the combination of Raman and QTM relaxation mechanisms.

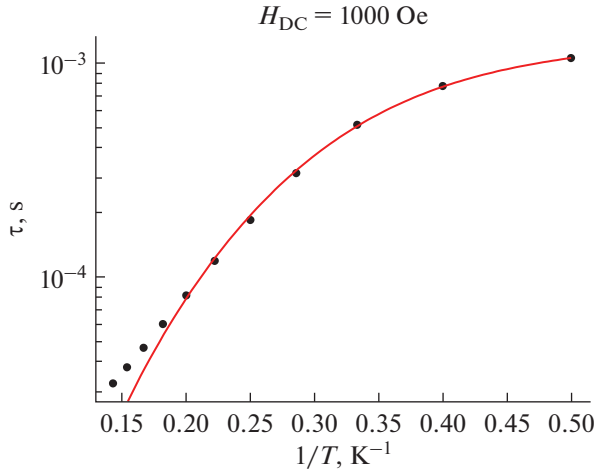

Fig. 12. The dependence of τ vs. $1/T$ for complex **II** under 1000 Oe dc-field. The solid red line is an approximation by the combination of Raman and QTM relaxation mechanisms.

It should be noted that an increase in the intensity of χ"(ν) signal was observed for **II** with an increase in temperature from 2 to 2.5 K (Fig. 10). This may originate from the collective behavior caused by the weak dipole-dipole or exchange interactions between the Gd^{3+} ions [20, 39–48].

The Orbach relaxation mechanism ($\tau = \tau_0 \times \exp(\Delta_{eff}/k_B T)$) for obtained Gd-containing complexes **I**, **II**, **IV**, and **V** is highly improbable. The values of τ_0 calculated from the high-temperature ranges of τ vs. $1/T$ graphs are not in the range of 1×10^{-10}–1×10^{-12}, which, according to the work [20] shows the non-Orbach origin of magnetic relaxation.

In the whole temperature ranges for complexes **I**, **II**, **IV**, and **V**, a cooperative contribution of Raman ($\tau_{Raman}^{-1} = C_{Raman} T^{n\_Raman}$) and QTM ($\tau_{QTM}^{-1} = B$) relaxation mechanisms was found to be the most appropriate. The best approximation parameters are given in Table 3. Low Raman exponents have been suggested to arise from an acoustic-optic two-phonon process [48].

Thus, a series of five Gd thiocyanate complexes was obtained, supplementing a number of similar families known for Y, Eu, and Dy. The study of a group of complexes for each complexing metal ion revealed general tendencies and specific features of the REE cations. The Y compounds provided a good single-crystal data base, which has formed a basis for the identification of the lanthanide families, while the Eu compounds has demonstrated photoluminescence features, and all the complexes of the Dy family has exhibited the properties of single-molecule magnets, the values of the magnetization reversal barriers of which were related to the structural features of the complexes.

D and *E* parameters, which characterize the splitting in zero field and the orthorhombicity of the system, are good markers that allow to evaluate the possibility of observing slow magnetic relaxation in the complexes. To reduce the relaxation rate of the system, it is necessary to maximize the absolute value of *D* parameter (which leads to an increase in the splitting between the levels), as well as to minimize *E* parameter (which leads to a decrease in the probability of relaxation by the direct mechanism). In this case, to observe slow magnetic relaxation, it is necessary that the *D* parameter values should be negative. It should be noted that a decrease in the values of *E* parameter below a certain value (~0.008 cm^{-1}) no longer affects

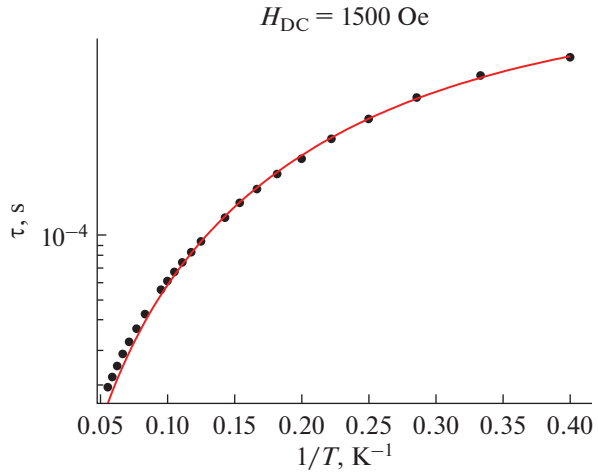

Fig. 13. The dependence of τ vs. $1/T$ for complex **V** under 1500 Oe dc-field. The solid red line is an approximation by the combination of Raman and QTM relaxation mechanisms.

Table 3. The parameters of the best approximation of the experimental dependences τ vs. $1/T$ of complexes **I**, **II**, **IV**, and **V** upon relaxation by the Raman and QTM mechanisms

Relaxation mechanism	Complex	**I**	**II**	**IV**	**V**
Raman	C_{Raman}, s^{-1} $K^{-n_{Raman}}$	0.30 (±0.03)	9 (±2)	1.6 (±0.2)	102 (±9)
	n_{Raman}	3.71 (±0.05)	4.4 (±0.1)	3.47 (±0.07)	2.21 (±0.05)
QTM	B, s^{-1}	87.4 (±0.9)	746 (±21)	300 (±5)	696 (±40)

the relaxation of the system as significantly as a change in the parameter D. To achieve the best relaxation characteristics (the highest magnetization reversal barrier) in isostructural Dy complexes, it is necessary that the values of the SG parameters of Gd complexes should be in the ranges determined by the values $D > 0.06$; $E < 0.008$ cm^{-1}. To clarify the boundaries of admissible parameter values, a significant expansion of the range of objects of this kind of research is required.

SUPPLEMENTARY INFORMATION

The online version contains supplementary material available at https://doi.org/10.1134/S1070328423601413.

ACKNOWLEDGMENTS

The authors are grateful to A.V. Gavrikov for recording the IR spectra. This research was performed using the equipment of the JRC PMR IGIC RAS.

FUNDING

This work was supported by the Russian Science Foundation, project no. 22-23-00574.

CONFLICT OF INTEREST

The authors of this work declare that they have no conflicts of interest.

REFERENCES

1. Shi, J.-M., Liu, Z., Xu, H.K., et al., *J. Coord. Chem.*, 2007, vol. 60, no. 15, p. 1637.
2. Lin, S.-Y., Wang, C., Zhao, L., et al., *Dalton Trans.*, 2015, vol. 44, p. 223.
3. Petrosyants, S.P., Dobrokhotova, Zh.V., Ilyukhin, A.B., et al., *Eur. J. Inorg. Chem.*, 2017, vol. 29, p. 3561.
4. Petrosyants, S.P., Ilyukhin, A.B., Gavrikov, A.V., et al., *Inorg. Chim. Acta*, 2019, vol. 486, p. 499.
5. Petrosyants, S.P., Babeshkin, K.A., Ilyukhin, A.B., et al., *Russ. J. Coord. Chem.*, 2021, vol. 47, p. 244. https://doi.org/10.1134/S1070328421040060
6. Petrosyants, S.P., Dobrokhotova, Zh.V., Ilyukhin, A.B., et al., *Inorg. Chim. Acta*, 2015, vol. 434, p. 41.
7. Ghose, M., Banerjee, S., Patra, S., Mukherjea, K.K., et al., *J. Lumin.*, 2016, vol. 180, p. 224.
8. Dobrokhotova, Zh.V., Petrosyants, S.P., Ilyukhin, A.B., et al., *Inorg. Chim. Acta*, 2017, vol. 456, p. 76.
9. Nockemann, P., Thijs, B., Postelmans, N., et al., *J. Am. Chem. Soc.*, 2006, vol. 128, p. 13658.
10. Ohaion, T., Kalisky, Y., Ben-Eliyahu, Y., et al., *Eur. J. Inorg. Chem.*, 2013, vol. 20, p. 3477.
11. Rogers, R.D., Zhang, J., Bauer, C.B., et al., *J. Alloys Compd.*, 1997, vol. 249, nos. 1–2, p. 41.
12. Cotton, S.A., Franckevicius, V., How, R.E., et al., *Polyhedron*, 2013, vol. 22, p. 1489.
13. Savard, D. and Leznoff, D.B., *Dalton Trans.*, 2013, vol. 42, p. 14982.
14. Naomi, M., Toshio, T., and Ouchi, A., *Bull. Chem. Soc. Jpn.*, 1990, vol. 63, no. 2, p. 620.
15. Matsumoto, F., Matsumura, N., and Ouchi, A., *Bull. Chem. Soc. Jpn.*, 1989, vol. 62, no. 6, p. 1809.
16. Bogani, L. and Wernsdorfer, W., *Nat. Mater.*, 2008, vol. 7, p. 179.
17. Sanvito, S., *Chem. Soc. Rev.*, 2011, vol. 40, p. 3336.
18. Mannini, M., Pineider, F., Sainctavit, P., et al., *Nat. Mater.*, 2009, vol. 8, p. 194.
19. Baldoví, J.J., Cardona-Serra, S., Clemente-Juan, J.M., et al., *Inorg. Chem.*, 2012, vol. 51, p. 12565.
20. Petrosyants, S.P., Babeshkin, K.A., Ilyukhin, A.B., et al., *Magnetochemistry*, 2023, vol. 9, p. 31.
21. Coutinho, J.T., Monteiro, B., and Pereira, L.C.J., *Ln(III)-Based SIMs*, Elsevier, 2018, p. 233.
22. Guo, Y.-N., Xu, G.-F., Guo, Y., and Tang, J., *Dalton Trans.*, 2011, vol. 40, p. 9953.
23. Roessler, M.M. and Salvadori, E., *Chem. Soc. Rev.*, 2018, vol. 47, p. 2534.
24. Goodwin, C.A.P., Reta, D., Ortu, F., et al., *J. Am. Chem. Soc.*, 2017, vol. 139, p. 18714.
25. Goodwin, C.A.P., Ortu, F., Reta, D., et al., *Nature*, 2017, vol. 548, p. 439.
26. Wilson, R.E., Carter, T.J., Autilloa, M., and Stegman, S., *Chem. Commun.*, 2020, vol. 56, p. 2622.
27. *APEX2 and SAINT,* Madison: Bruker AXS Inc., 2007.
28. Sheldrick, G.M., *SADABS*, Göttingen: Univ. of Göttingen, 2014.

29. Sheldrick, G.M., *Acta Crystallogr., Sect. C: Struct. Chem.*, 2015, vol. 71, p. 3.
30. Petrosyants, S.P. and Ilyukhin, A.B., *Russ. J. Coord. Chem.*, 2014, vol. 40, p. 825. https://doi.org/10.1134/S107032841410008X
31. Coelho, A.A., *TOPAS, Version 4.2 (Computer Software)*, Brisbane: Coelho Software, 2009.
32. Belford, G.G., Belford, R.L., and Burkhaven, J.F., *J. Magn. Res.*, 1973, vol. 11, p. 251.
33. Rakitin, Yu.V., Larin, G.M., and Minin, V.V., *Interpretatsiya spektrov EPR koordinatsionnykh soedinenii* (Interpretation of EPR Spectra of Coordination Compounds), Moscow: Nauka, 1993.
34. Ilyukhin, A., Dobrokhotova, Zh., Petrosyants, S., and Novotortsev, V., *Polyhedron*, 2011, vol. 30, p. 2654.
35. Pawlak-Jarosz, N., Oczko, G., Starynowicz, P., and Kot, K., *J. Mol. Struct.*, 2018, vol. 1171, p. 396.
36. Banerjee, S., Ghose, M., Paul, S., et al., *J. Coord. Chem.*, 2016, vol. 69, no. 4, p. 604.
37. Kot, K. and Oczko, G., *Polyhedron*, 2018, vol. 146, p. 145.
38. Chilton, N.F., Anderson, R.P., Turner, L.D., et al., *J. Comput. Chem.*, 2013, vol. 34, p. 1164.
39. Babeshkin, K.A., Gavrikov, A.V., Petrosyants, S.P., et al., *Eur. J. Inorg. Chem.*, 2020, vol. 46, p. 4380.
40. Efimov, N.N., Koroteev, P.S., Gavrikov, A.V., et al., *Magnetochemistry*, 2016, vol. 2, p. 38.
41. Gavrikov, A.V., Efimov, N.N., Dobrokhotova, Zh.V., et al., *Dalton Trans.*, 2017, vol. 46, p. 11806.
42. Petrosyants, S.P., Ilyukhin, A.B., Efimov, N.N., et al., *Inorg. Chim. Acta*, 2018, vol. 482, p. 813.
43. Koroteev, P.S., Ilyukhin, A.B., Efimov, N.N., et al., *Polyhedron*, 2018, vol. 154, p. 54.
44. Mamontova, E., Long, J., Ferreira, R., et al., *Magnetochemistry*, 2016, vol. 2, p. 41.
45. Habib, F., Lin, P.-H., Long, J., et al., *J. Am. Chem. Soc.*, 2011, vol. 133, p. 8830.
46. Bilyachenko, A.N., Yalymov, A.I., Korlyukov, A.A., et al., *Chem. Eur. J.*, 2015, vol. 21, p. 1856.
47. Polyzou, C.D., Koumousi, E.S., Lada, Z.G., et al., *Dalton Trans.*, 2017, vol. 46, p. 14812.
48. Shrivastava, K.N., *Phys. Stat. Sol., B*, 1983, vol. 117, p. 437.